

Cite this: DOI: 10.1039/c1dt10319a

www.rsc.org/dalton

PAPER

Maghemite (hematite) core (shell) nanorods *via* thermolysis of a molecular solid of Fe-complex†

N. S. Chaudhari,^a S. S. Warule,^a S. Muduli,^b B. B. Kale,^{*a} S. Jouen,^c B. Lefez,^c B. Hannoyer^c and S. B. Ogale^{*b}

Received 24th February 2011, Accepted 20th May 2011

DOI: 10.1039/c1dt10319a

An Fe-metal complex with 2'-hydroxy chalcone (2'-HC) ligands [Fe(III) (2'-hydroxy chalcone)₃] is synthesized by a chemical route and is subjected to different thermal treatments. Upon thermolysis in air at 450 °C for 3 h the complex yields maghemite (γ -Fe₂O₃) nanorods with a thin hematite (α -Fe₂O₃) shell. X-Ray diffraction (XRD), Mössbauer spectroscopy, diffuse reflectance spectroscopy (UV-DRS), high resolution transmission electron microscopy (HR-TEM), field emission scanning electron microscopy (FE-SEM) and vibrating sample magnetometry (VSM) are used to characterize the samples. The stability of the ligand and the Fe-complex is further examined by using thermogravimetric/differential thermal analysis (TGA/DTA). We suggest a residual ligand controlled mechanism for the formation of an anisotropic nanostructure in a crumbling molecular solid undergoing ligand decomposition. Since the band gap of iron oxide is in the visible range, we explored the use of our core shell nano-rod sample for photocatalytic activity for H₂ generation by H₂S splitting under solar light. We observed high photocatalytic activity for hydrogen generation (75 ml h⁻¹).

1. Introduction

Nanometre-scale magnetic materials are scientifically interesting and technologically important for diverse fields such as biomedicine, magnetic recording, and spin electronics.¹⁻³ Phase and shape controlled facile and scalable synthesis of magnetic nanoparticles is therefore an important endeavour in the context of the emerging technologies. Uniformly sized quasi one dimensional (1-D) nanostructures such as nanowires, nanotubes and nanorods have received particular attention in this regard because of the unique properties derived from their dimensional anisotropy⁴ and their potential applications as functional building blocks for nano-devices. There are various strategies for obtaining quasi 1-D nanostructures that include the use of intrinsically anisotropic crystal structures, shape directing soft or hard templates, use of different coordinating ligands to control the growth rates of different crystal facets, the vapor-liquid-solid process, and the self assembly of spherical nanoparticles by oriented attachment.⁵

However, facile self propelled synthetic methods for the growth of anisotropic structures are not that abundant. In this article, we report the facile synthesis of iron oxide two-phase core shell type nanorods by low temperature thermolysis of a metal-complex [Fe(III) (2'-hydroxy chalcone)₃] and discuss the related chemistry and mechanisms. There have been several studies on nano-synthesis *via* decomposition of organometallic systems, but there is very little work employing metal complexes, such as the one used in this work. We believe and demonstrate that such complexes are in fact the better and a natural choice for oxide nanoparticle synthesis because of the in-built metal ion-oxygen coordination therein. We also demonstrate the applicability of the synthesized structure for solar photocatalytic H₂S splitting for hydrogen generation. It is well known that the catalytic properties are dependent on the morphology, particle size and surface area. We show that our nanorod type core shell catalyst shows higher photocatalytic activity as compared to previous reports.⁶

Among the various nanostructured materials magnetic nanoparticles have attracted growing interest owing to their unique properties and potential applications in various fields⁷⁻⁸ such as information storage, magnetic sealing, ferro-fluid technology, magneto-caloric refrigeration and catalysis, magnetically-assisted drug delivery, magnetic resonance imaging (MRI) contrast enhancement, hyperthermia, bio-molecular separation, and isolation/recycling of expensive catalysts. Iron oxides such as magnetite (Fe₃O₄) and maghemite (γ -Fe₂O₃) are considered to be the most useful materials for these technological applications because of their biocompatibility, high magnetic transition temperature and high saturation magnetization.⁹ The non-magnetic hematite is also of great interest for photocatalysis,⁶ electrode material in

^aCenter for Materials for Electronics Technology, Department of Information Technology, Govt. Of India, Panchwati, Off Pashan Road, Pune, 411 008, Pune, INDIA. E-mail: kbbbl@yahoo.com, bbkale@cmet.gov.in; Fax: +91-20-2589 8085; Tel: +91-20-2589 8390

^bPhysical and Materials Chemistry Division, National Chemical Laboratory, Dr Hombi Bhabha Road, Pashan, Pune, 411 008, Pune, INDIA. E-mail: sb.ogale@ncl.res.in, satishogale@gmail.com; Fax: +91-20-2590-2636; Tel: +91-20-2590-2260

^cGroupe de Physique des Matériaux, Université de Rouen, GPM UMR 6634 CNRS, Institut des Matériaux de Rouen, 76801, St Etienne du Rouvray CEDEX, FRANCE

† Electronic supplementary information (ESI) available. See DOI: 10.1039/c1dt10319a

lithium ion batteries, and for gas sensor development.^{10–11} The oxidation kinetics and transformations of different phases of iron oxide have been well documented.¹² Various approaches such as anodic aluminium oxide (AAO) hard template process,¹³ Lecithin soft template process,^{14–15} and redox methods,^{16–17} have been developed for the preparation of the quasi 1D forms of magnetic materials. However these methods are complex, hence alternate facile synthesis routes are still being pursued.

2. Results and discussion

Fig. 1 summarizes the X-ray diffraction (XRD) data for various cases of interest. The curve 'a' corresponds to the XRD of the molecular solid formed by the Fe-complex, while curve 'b' shows the result for the Fe-complex annealed at 375 °C for 2 h. The XRD of the Fe-complex powder shows fairly sharp line structure indicating that it acquires crystallinity in the solid state. This feature in most molecular solids is ascribed to macromolecular organization through Van der Waals interactions. The 375 °C annealed sample shows a broad hump in the 2θ range of 10–30°, *i.e.* over the same range (including the primary peak position) as the prominent peak structure in the XRD of the Fe-complex. This, along with the weight loss revealed by the TGA measurements discussed later, indicates that around 375 °C disordering of the molecular lattice takes place, due to the loss of some ligand sections by decomposition. Interestingly in the curve 'b' some new peaks with low intensity are also seen that are not present in the XRD of the Fe-complex, and these correspond to the (311) and (400) planes of the spinel phase of iron oxide. This indicates that the decomposition of ligand and iron oxide phase formation take place concurrently, implying a direct connection between the two.

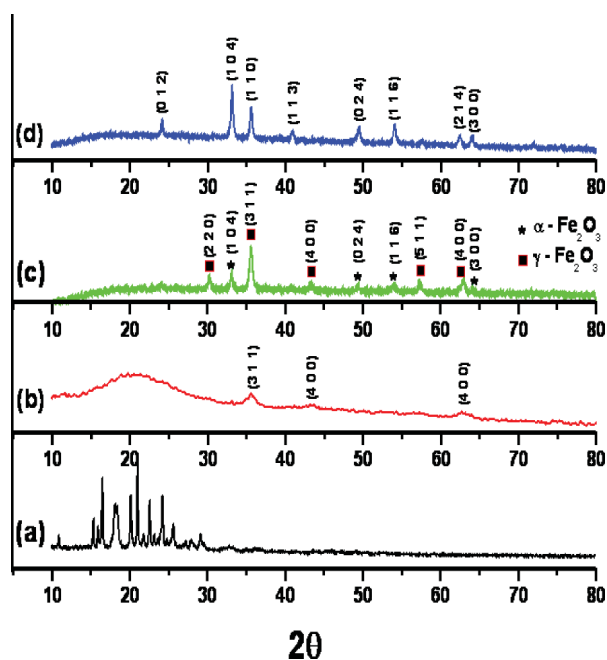


Fig. 1 XRD spectra of samples Fe-complex (a) and Fe-complex annealed at 375 °C for 2 h (b), 450 °C for 3 h (c) and 500 °C for 3 h (d) in air.

Curve 'c' of Fig. 1 reveals the structure of the decomposed end product of [Fe(III) (2'-HC)₃] upon annealing at 450 °C for

3 h which was found to be magnetic at room temperature. The primary peaks can be easily identified with the spinel phase. The magnetic forms of iron oxide that are spinel are Fe₃O₄ and γ -Fe₂O₃. It is well known however that only on the basis of routine XRD it is difficult to ascertain the presence of magnetite or maghemite, since the two have very closely matched XRD patterns as per the reported data [(magnetite (JCPDS 85-1436) and maghemite (JCPDS-39-1346)]. Optical techniques can reveal the difference, and as shown later the phase in our case is found to be maghemite. In addition to the spinel phase, characteristic peaks corresponding to α -Fe₂O₃ can also be noted in Fig. 1(c), but their intensities are relatively lower. The extra heat released during the exothermic decomposition,⁶ may be responsible for the conversion of a thin surface layer of the spinel phase to α -Fe₂O₃. For the samples formed by thermolysis at 500 °C for 3 h Fig. 1d, the XRD pattern matched very well with that of α -Fe₂O₃ (standard cards, JCPDS 33-0664), suggesting that the α -Fe₂O₃ forms *post facto* via the initial spinel formation. The presence of the stable and non-ferromagnetic 3+ surface oxide on the ferrimagnetic spinel phase offers specific advantages. For instance, the non-ferromagnetic coating will avoid agglomeration of nanoparticles due to weakening of the magnetic contact interactions. Moreover, hematite is itself a known catalyst,^{18–19} and when supported on a magnetic core, it can be easily separated from the catalytic medium magnetically. In the catalysis context there could be interesting possibilities of mixed valent states afforded by the Fe₃O₄ core.

In order to investigate the phase transformation with respect to heating time we annealed the Fe-complex at a constant temperature of 450 °C for different time durations namely 60, 90, 180, 240 and 300 min. Fig. 2a–e show the XRD patterns of the respective samples. The XRD pattern of the sample heated for 60 min (Fig. 2a) shows a hump at 20° representing residual carbon along with some peaks corresponding to the γ -Fe₂O₃ phase. The carbon is seen to get reduced with further evolution of the γ -Fe₂O₃ phase in the case of the sample heated for 90 min (Fig. 2b). The formation of the α -Fe₂O₃ phase is clearly seen to have ensued in the case of the sample annealed for 180 min (Fig. 2c) along with the

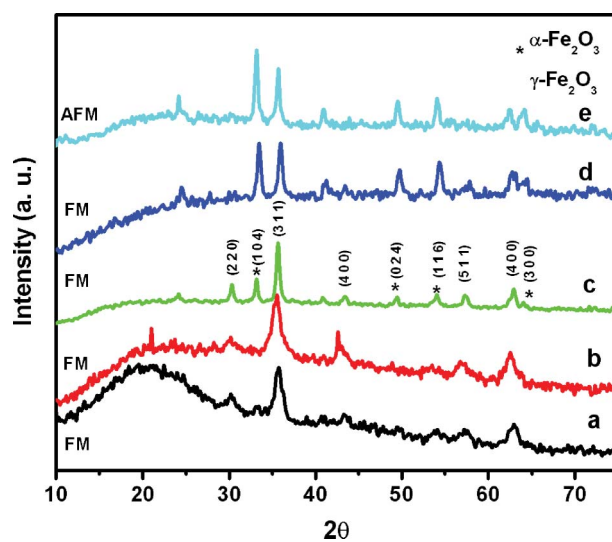


Fig. 2 XRD spectra of Fe-complex annealed at 450 °C for (a) 60 min, (b) 90 min, (c) for 180 min, (d) 240 min and (e) 300 min. (FM = ferromagnetic, AFM = antiferromagnetic).

presence of the γ - Fe_2O_3 phase (sharper lines). When the heating time is further increased to 240 min the maghemite contribution begins to decrease with enhancement of the hematite contribution (Fig. 2d). As marked on the curves in the figure all the samples heated for 240 min or less are ferromagnetic (pulled by a magnet), confirming the presence of the ferromagnetic gamma phase, which should be in the core because the oxidation (leading to hematite contribution) starts from the outer surface. Upon increasing the duration of heating further to 300 min, pure hematite is obtained. This study shows that the heating time is an important factor for getting a specific (core) shell (γ - Fe_2O_3) α - Fe_2O_3 structure.

Since an electronic spectrum can provide valuable information concerning the environment of the ferrous/ferric ions the same was recorded and analyzed. It consists of the electronic transitions localized at the FeO_6 co-ordination sites, and also reveals the phenomena resulting from the interactions between adjacent iron cations. Fig. 3a–c shows the visible and near infrared diffuse reflectance spectra (DRS) for the ligand, Fe-complex and the Fe-complex annealed at 450 °C for 3 h. The absorption bands at $\sim 11\,000\text{ cm}^{-1}$ and $15\,000\text{ cm}^{-1}$ in Fig. 3b and 3c are assigned to the transitions ${}^6\text{A}_1({}^6\text{S})$ to ${}^4\text{T}_1({}^4\text{G})$ and ${}^6\text{A}_1({}^6\text{S})$ to ${}^4\text{T}_2(\text{G})$, respectively, associated with ligand field transition of Fe^{3+} in octahedral sites.²⁰ Absence of an absorption band at 7000 cm^{-1} and a low absorption level between 4000 – 25000 cm^{-1} strongly implies that the spinel sample has Fe^{3+} state only, because concurrent presence of Fe^{2+} and Fe^{3+} must necessarily lead to the signatures stated here that result from charge transfer between Fe^{2+} and Fe^{3+} . Our spinel phase is thus γ - Fe_2O_3 (which has only Fe^{3+}) and not Fe_3O_4 (which has both Fe^{2+} and Fe^{3+}). It may be recalled that XRD data cannot distinguish between the two spinels, but as shown here, the optical data does.

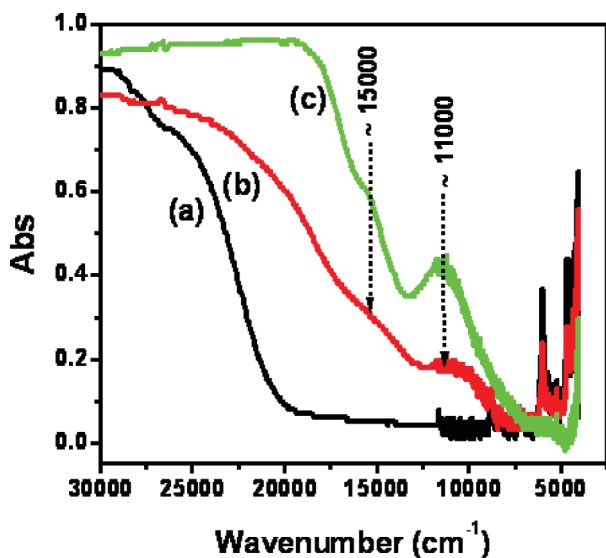


Fig. 3 Visible and near infrared diffuse reflectance spectra of (a) ligand, (b) Fe-complex, and (c) Fe-complex annealed at 450 °C for 3h.

In the case of the IR spectrum of the sample annealed at 450 °C (Fig. 4) all the bands observed in the range of 400 – 800 cm^{-1} correspond to the stretching vibrations of Fe–O bonds. On the other hand, in the case of the sample annealed at 375 °C such well developed Fe–O signatures are not seen. Moreover other signatures representing organic groups are seen to be present which

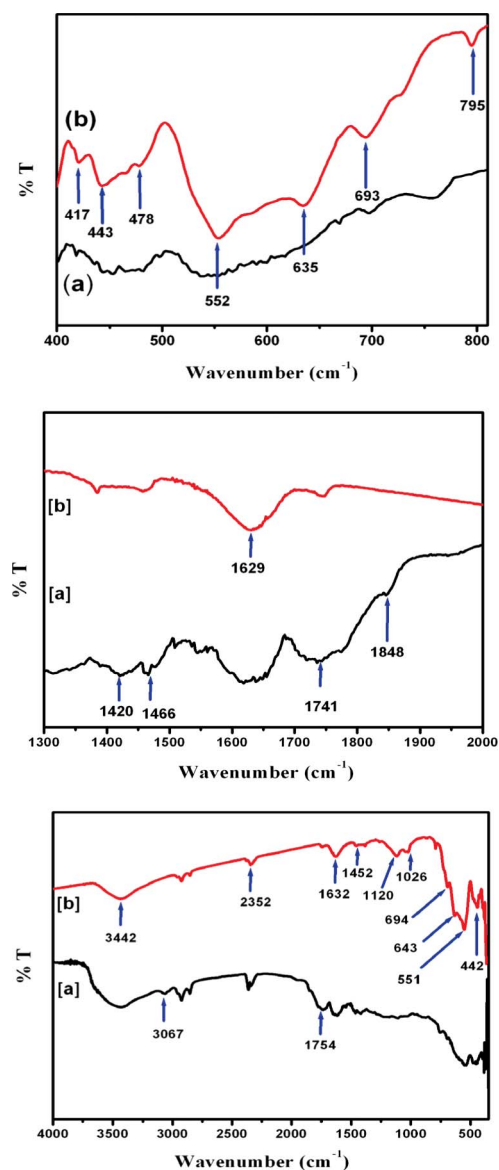
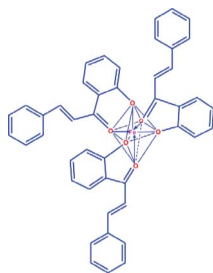


Fig. 4 FTIR spectra of the Fe-complex annealed at 375 °C (curves marked a) and at 450 °C (curves marked b) at different frequency ranges.

implies incomplete oxidation. The absorption band at 3442 cm^{-1} observed in both the cases is due to the typical surface hydration.²⁰ The band observed at 1629 cm^{-1} is also due to the hydrates (relating to O–H bonding).²¹ The water of crystallization can be found from this latter bond and it is helpful in elucidation of the crystal structure. Some intense bands are observed in the 375 °C sample (Fig. 4) at 3067 cm^{-1} ($=\text{C-H}$ stretching), 1400 – 1500 cm^{-1} (C-H stretching), and 1600 – 1850 cm^{-1} (C=O and C=C bonds). These indicate that organic residue remains for such low temperature treatment. The absence of Fe–O signatures and presence of organic groups in the sample synthesized by annealing Fe-complex at 375 °C implies that at this temperature partial decomposition of complex does take place, but only an intermediate product is formed which needs higher temperature (450 °C) to further develop into Fe_2O_3 .

The fact that the observed Fe–O coordination in the Fe-complex is octahedral (6 oxygen atoms) together with the



Scheme 1 Structural formula of $[\text{Fe}(\text{III})(2'\text{-HC})_3]$ complex.

Scheme 1 representing Fe-ligand attachment implies that three ligands should be bound to one FeO_6 octahedron, as shown. This configuration would however require Fe to have 3+ valence state. This is clearly borne out by the Mössbauer spectroscopy data discussed next.

Fig. 5 shows the Mössbauer spectroscopy data for the Fe-complex (a), the same annealed at 375 °C for 2 h (b) and at 450 °C for 3 h (c). The corresponding hyperfine interaction parameters are summarized in Table 1. The average value of isomer shift (0.35 mm s^{-1}) observed for the Fe-complex (Fig. 5a) implies that Fe is in 3+ high-spin state and essentially confirms the structure of the Fe-complex shown in Scheme 1. Interestingly, the isomer shift for the case of the Fe-complex annealed at 375 °C for 2 h (Fig. 5b) also shows Fe in 3+ state. It is well-known that the isomer shift value varies with bond length and Fe–O–Fe bond angle. As will be discussed later based on the TGA analysis, there is significant weight loss of the sample as this temperature is reached. This weight loss is clearly due to molecular scission or breaking. The Mössbauer result then suggests that the thermal splitting of molecular structure occurs in such a way that 3+ state of Fe is

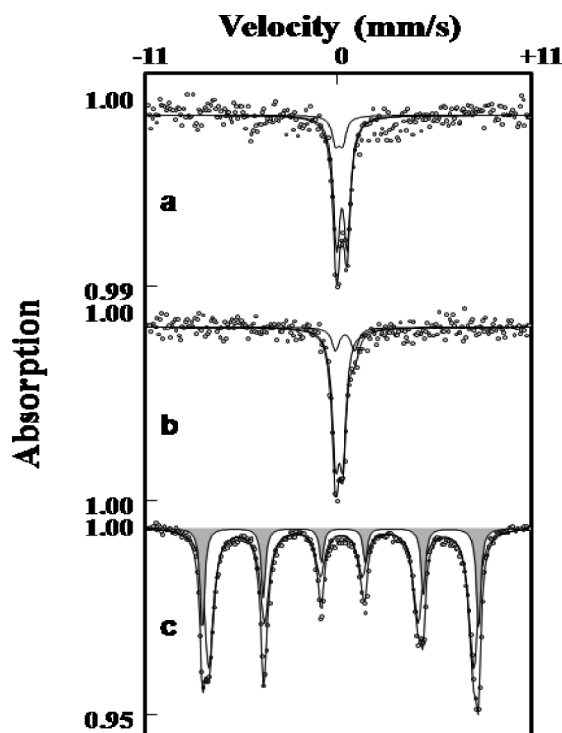


Fig. 5 Mössbauer spectra of (a) Fe-complex (b) Fe-complex annealed at 375 °C and (c) Fe-complex annealed at 450 °C.

Table 1 Mössbauer parameters

Sample	δ (mm s^{-1})	2ϵ or Δ (mm s^{-1})	B_{hf} (T)
a	0.20	0.41	—
	0.37	0.62	—
b	0.20	0.41	—
	0.53	1.10	—
c	0.33	0.00	48.8
	0.37	-0.17	50.9

not changed. The final iron oxide compound thus evolves from the modified molecular complex wherein Fe is in the 3+ state. The data for the sample annealed at 450 °C for 3 h (Fig. 5c) show a hyperfine split sextet indicating magnetic state. The fitted parameters for this case shown in Table 1 bring out the presence of $\gamma\text{-Fe}_2\text{O}_3$, as the main phase with iron in the trivalent state and zero value of quadrupole shift (2ϵ) showing cubic symmetry, with admixture of $\alpha\text{-Fe}_2\text{O}_3$ (gray coloured sextet with its characteristic quadrupole shift) in agreement with the XRD data.

Fig. 6a depicts a TEM image of the Fe-complex annealed at 450 °C for 3 h showing the nanorod configuration of the product of thermolysis. The average diameter and length of the rod are about 13 nm and 200 nm, respectively. From the electron diffraction pattern (Fig. 6b), all d_{hkl} values (indicated in white) match with the $\gamma\text{-Fe}_2\text{O}_3$ phase. Also present are weak diffractions (indicated in red) corresponding to the $\alpha\text{-Fe}_2\text{O}_3$ phase. These data corroborate well with the XRD, Mössbauer and Raman observations (discussed later). A typical result of our high resolution TEM imaging is shown in Fig. 6c. Although the presence of a shell can be noticed the contrast is not sufficient from the standpoint of clarity. This is understandable because the two oxides ($\gamma\text{-Fe}_2\text{O}_3$ and $\alpha\text{-Fe}_2\text{O}_3$) have the same elements (forbidding the elemental Z contrast) and the densities of the two phases are also not too different ($\sim 4.9 \text{ g cm}^{-3}$ for maghemite and $\sim 5.3 \text{ g cm}^{-3}$

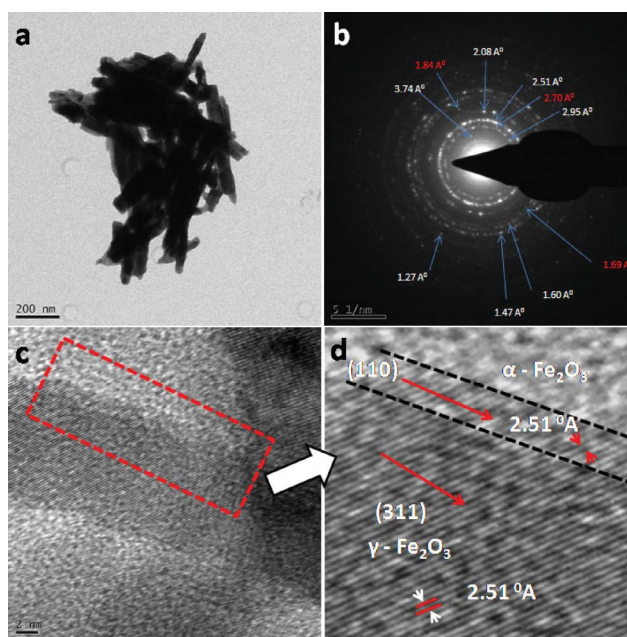


Fig. 6 (a) Typical TEM images of the sample heated at 450 °C for 3 h, (b) is the corresponding electron diffraction pattern and (c–d) HRTEM images of the same sample.

for hematite). As seen from the enlarged image of Fig. 6d, the d -value for the (311) plane ($d_{(311)} = 2.51 \text{ \AA}$) of the maghemite (core) phase (highest intensity peak in the XRD data, hence most clearly imaged plane in HRTEM) matches very well with the d -value for the (110) plane system of the hematite (shell) phase. Hence upon oxidation the latter appears to grow epitaxially on the core phase as shown.

Fig. 7 shows the Raman spectrum of the solid phase formed after annealing at $450 \text{ }^\circ\text{C}$ for 3 h, along with a spectrum for a maghemite sample recorded under the same conditions. Low laser power density was used to record the spectrum because Raman spectra of iron oxides are known to be sensitive to laser power. The laser power was reduced using a filter D3 as designated Horiba to work with less power *i.e.* 0.7 mW. The maghemite sample was run to ensure that the hematite shell formation is not taking place during the Raman experiment and is indeed formed in the synthesis process itself. A standard spectrum of $\alpha\text{-Fe}_2\text{O}_3$ (hematite) is included in the figure for comparison. The synthesized inorganic phase clearly shows Raman features of both hematite (marked *) and maghemite (marked \downarrow) phases. The contribution of hematite is of course much stronger than maghemite. This strongly supports the suggested maghemite (hematite) core (shell) nature of the particles, because the Raman contribution of the surface shell is known to be strongly enhanced as compared to the core contribution. The Raman spectrum of the annealed sample shows all those peaks which are present in the standard Raman spectrum of hematite (as shown in Fig. 7) while the Raman signals associated with maghemite appear as broad features at 502 , 665 and 716 cm^{-1} .

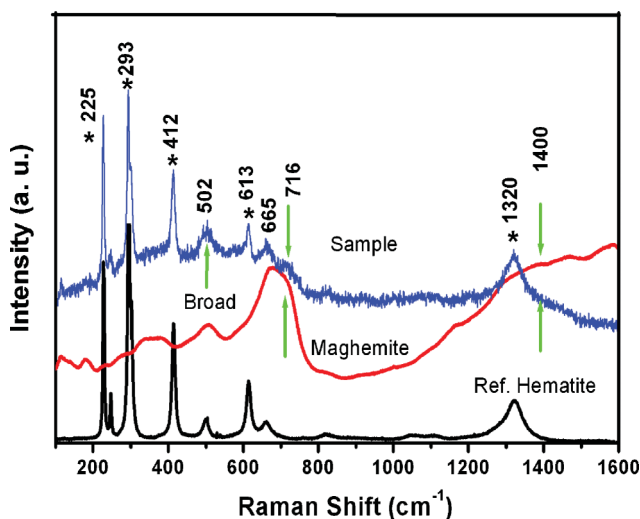


Fig. 7 Raman spectra of the (a) Fe-complex annealed at $450 \text{ }^\circ\text{C}$ for 3 h (b) maghemite sample and (c) standard $\alpha\text{-Fe}_2\text{O}_3$ (hematite).

Fig. 8 displays the hysteresis loop for the maghemite (hematite) core (shell) nanorod sample, which shows magnetic saturation (M_s) value of 43 emu g^{-1} . The decrease in M_s compare to bulk $\gamma\text{-Fe}_2\text{O}_3$ (74 emu g^{-1}) is likely due to nano size and can be partly attributed to the mass of antiferromagnetic $\alpha\text{-Fe}_2\text{O}_3$ surface layer and also possibly to spin disordering near the interface.²⁵⁻²⁶ The insets of Fig. 8 show the loop at 10 K and the field cooled/zero field cooled (ZFC/FC) magnetization data. The applied field used for FC procedure is 50 Oe. The blocking temperature is close

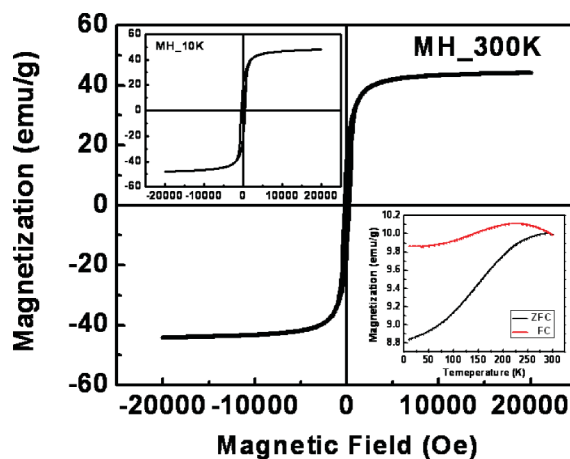


Fig. 8 VSM spectra of annealed Fe-complex at $450 \text{ }^\circ\text{C}$ for 3 h sample.

to room temperature which is consistent with the size of the nanorods.^{20,27} The excellent magnetic properties combined with the non-magnetic surface shell should find interesting applications for such nanoparticles.

The FE-SEM images were also recorded for the as-synthesized Fe-complex, the Fe-complex annealed at $375 \text{ }^\circ\text{C}$ for 2 h and the Fe-complex annealed $450 \text{ }^\circ\text{C}$ for 3 h (Fig.9). In one case the complex and its annealed powders were simply examined in the powder form, while in another case the same were examined in the form of a film coated on silicon substrate and then annealed. The

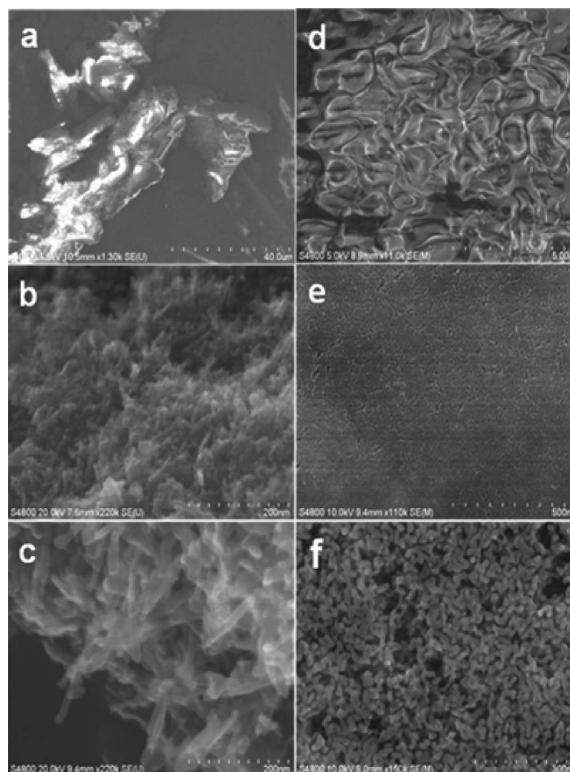


Fig. 9 FE-SEM micrographs of (a, d) Fe-complex, (b, e) Fe-complex annealed at $375 \text{ }^\circ\text{C}$ for 2 h, and (c, f) Fe complex annealed at $450 \text{ }^\circ\text{C}$ for 3 h. The images (a, b, c) correspond to powder form and the images (d, e, f) correspond to the case when the powder was dissolved in chloroform and then the dried film of the complex was examined.

coating was performed by making a solution of the Fe-complex in chloroform and drop casting the same on the silicon substrate. The left panels show the images for the powder case, while the right panels show the images for the film case. It is important to mention here that in the powder case, it was difficult to take the images because the sample was getting affected by the imaging beam, at least in the case of the as-synthesized Fe-complex. A crumpled sheet-like but dense morphology is apparent in the case of the Fe-complex film coated on silicon, while larger buckled sheets are seen in the case of Fe-complex powder sample. Upon heating at 375 °C for 2 h, the morphology is seen to evolve significantly with tiny rod like patterns developing in both cases, although the length scales are different possibly due to the differences in the quantity of the material and the thicknesses of layers in the two cases. It is important to note from these central panels that the seeds of rod-like growth are formed right at this stage, although as seen from Fig. 1b, the iron oxide phase does not develop. Moreover other techniques revealed that this material also has carbon content, implying that further heating is necessary. Upon heating further at 450 °C for 3 h, the rod dimensions are clearly seen to get enhanced significantly, suggesting coarsening of the original nanostructures. It is interesting to note that the nanostructures are fairly uniform, more so in the case of the coated film. We believe that this low temperature Fe-complex thermolysis procedure can be effective in making interesting composite materials and films.

To observe the effect of heating time on the particle morphology the samples prepared at 450 °C at a heating rate 15 °C per min for different hold times (30, 90, 150 and 180 min) at 450 °C. These were characterized using the FESEM technique. The 30 min heat treated sample (Fig. 10a) clearly shows initiation of the growth of nanorods (~13 nm diameter), while in the case of the 90 min heated sample (Fig. 10b) aligned and connected particulate features are noted. This suggests that in the sample heated for a shorter duration carbon is still present and is gradually removed to yield iron oxide phase(s). When the time is extended to 150 min the particles (which should now be primarily iron oxide without carbon) begin to sinter together in the form of rods (Fig. 10c). Finally uniform nanorods are obtained after heating for 180 min

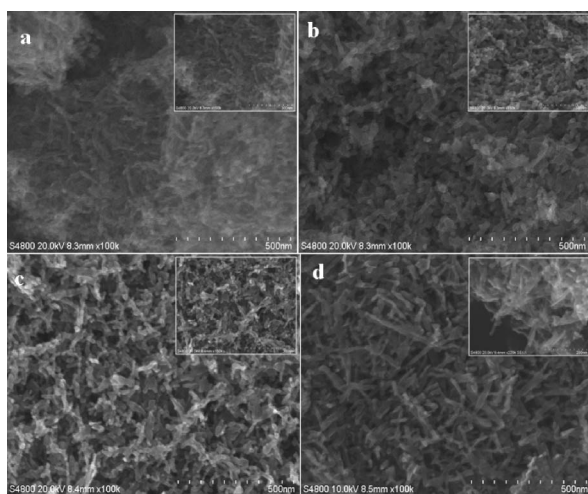


Fig. 10 FESEM micrographs for different durations of heating (a) 30 min, (b) 90 min, (c) 150 min and (d) 180 min at 450 °C for heating rate of 15 °C per min (inset shows magnified micrographs).

(Fig. 10d), having almost the same diameter and a length of ~200 nm. The XRD patterns of Fig. 2 also confirm the complete formation of well crystalline nanorods when the heating time is 180 min.

Fig. 11 shows the FESEM micrographs of the samples synthesized for different heating rates (1, 5, 10 and 15 °C per min) with final heating at 450 °C for 3 h (corresponding XRD patterns shown in SI-1†). It is observed that the morphology evolves from particulate-like to rod-like with the increase of the heating rate. In the cases of samples heated at 1 °C per min and 5 °C per min particles with a diameter of ~10 nm (Fig. 11a) and ~13 nm (Fig. 11b), respectively, are seen. In the case of the sample heated at 10 °C per min rod formation is initiated (Fig. 11c). Finally, uniform rod formation with average diameter ~13 nm is obtained for the heating rate of 15 °C per min (Fig. 11d).

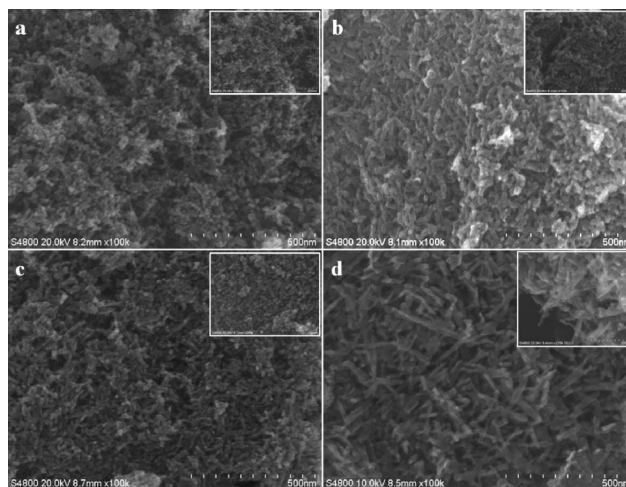
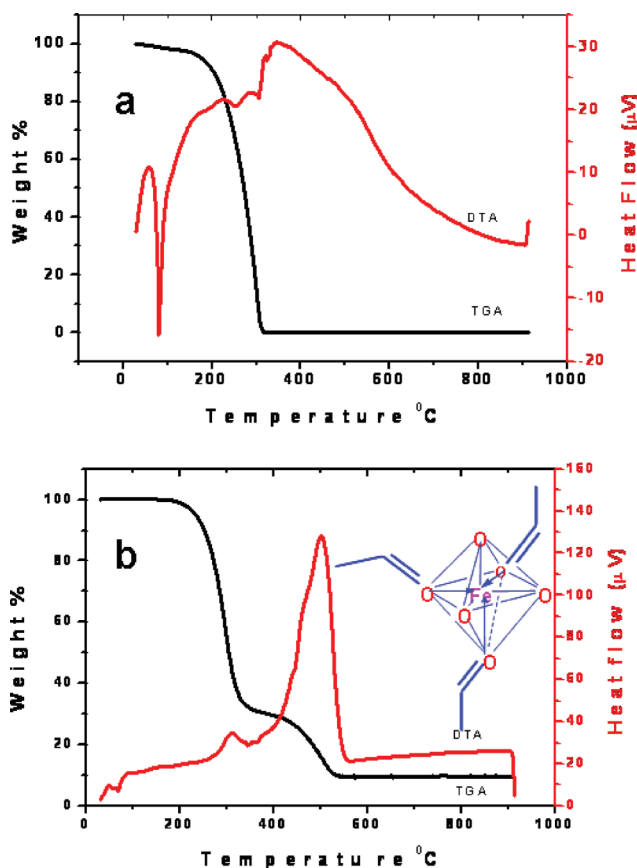


Fig. 11 FESEM micrographs for different heating rates (a) 1 °C, (b) 5 °C, (c) 10 °C and (d) 15 °C per min leading to 450 °C (inset shows magnified micrographs).

To explore the chemistry of thermolytic transformation, TGA–DTA (Differential Thermal Analysis) study of ligand 2'-HC (organic compound) and its Fe-complex was performed in the temperature range from room temperature to 900 °C in air. The DTA curve for the ligand case (Fig. 12a) exhibits two endothermic peaks in the temperature range of 75 °C to 350 °C. The first endothermic peak appearing at 81 °C can be attributed to the melting of the ligand, because there is no weight loss observed at this temperature in the TG curve.²⁸ The second endothermic peak observed in between 250 °C to 305 °C is attributed to the 100% decomposition of the ligand. The DTA curve of the Fe-complex (Fig. 12b) shows one endothermic peak at 72 °C implying melting of the complex. Another exothermic peak is seen at 313 °C, suggesting partial thermolysis of the organic section of the ligand. Finally, one sharp and intense exothermic peak is observed at ~500 °C, indicating complete decomposition of ligand and formation of stable iron oxide. Above 550 °C slow oxygen uptake is also notable. The thermogravimetric analysis of Fe-complex in air indicates that it decomposes in a stepwise manner in contrast to the sharp and single step decomposition of the ligand. The energy of activation for each step during the weight loss was calculated by Coats and Redfern method.²⁹ Table 2 presents the stepwise weight loss and energy of activation for that step at the respective temperature.

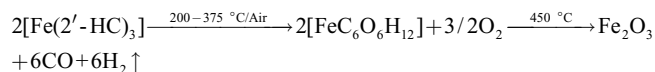
Table 2 Thermogravimetric analysis of ligand and Fe-complex

Name of comp.	Step-1 st			Step-2 nd		
	Temp/°C	Wt. loss (%)	E _a /kcal mol ⁻¹	Temp./°C	Wt. loss (%)	E _a /kcal mol ⁻¹
Ligand (2'-HC)	40–320	100	16	—	—	—
Fe-complex	200–375	70	54	375–500	19	138

**Fig. 12** TG and DTA curves of (a) ligand (b) Fe-complex.

The energy for the ligand is very much less (16 kcal mol⁻¹) than the energy of activation for the first step in Fe-complex (54 kcal mol⁻¹). This implies that the stability of ligand increases in the complex due to the chelating effect. TGA of Fe-complex indicates that it is stable up to 200 °C. During the first step about 70% weight loss observed over the temperature range of 200 °C to 375 °C. This weight loss is obtained due to the pyrolysis of organic residue in the ligand section. The total relative atomic mass of Fe-complex molecule corresponds to 725 (relative to C12). With the loss of 70% of its mass, the ~30% residual mass is 218. This closely corresponds to the relative mass of the molecule (236) shown in the inset of the TGA curve, wherein the aromatic portions are totally removed. The formula for this molecule stands as FeC₆O₆H₁₂. Thus the final transformation to the iron oxide phase(s) takes place by the decomposition of this intermediate. The overall weight loss of the starting Fe-complex to the final step is ~89% which corresponds very closely to the relative atomic mass of Fe₂O₃, the stoichiometry of final phase formed.

The proposed reaction inferred from the TGA curve is:



Possible mechanism

The present work on nanorod synthesis (anisotropic growth) represents a case of solid–solid phase transformation and related chemistry involving a molecular solid with a ligand configuration. These are basically Van der Waals solids bound through dispersion forces. It is useful to state here that although the complex melts at low temperature before undergoing decomposition, it forms a solid containing carbon at about 375 °C and this solid act as a precursor system for the final product evolution (maghemite/hematite core shell).

In our case the original solid is clearly a crystalline one as reflected by a well defined XRD pattern. As the thermal treatment proceeds some mass is lost due to the breaking and escaping ligands as shown by the TGA analysis, and an intermediate amorphous molecular solid gets formed with shorter ligands (with a possible configuration as shown in the inset of Fig. 12b). This configuration could morph into other closer ones such as, for example, a nonacarbonyl which has comparable mass, but we do not have a proof of this possibility. In either case we have an octahedral configuration with short ligands. Thermolysis must ensue a crumbling sequence wherein escape of sections of broken ligands must render rearrangement of residual ligands for minimization of energy. It is to be remembered that many such solids are not expected to have high thermal conductivity and hence the crumbling sequence would start and grow from the regions which are in thermal contact with the heater, unless concurrent bulk heating strategies such as microwave heating are adopted. This in itself gives directionality to the synthesis process which may have some contribution to the development of anisotropy. Also, as the transient pores develop due to the escape of broken ligand sections, network strains can enforce directionality through pore coordination and axial growth similar to the advancement of a crack tip in a cracking pattern in the process of film formation from drying colloids. Indeed in the FESEM picture for the case of the nanorod film such a precursor cracking pattern seems apparent and the nanorods are seen to evolve along the cracks. Also, the octahedral ligand structure has a peculiarity that the full departure of one ligand can lead to a configuration which will naturally tend to juxtapose with another similar configuration through reorientation so as to maximize the dispersion force, thereby promoting a linear configuration. This would, intrinsically, force the FeO₆ octahedra to enjoin along a linear direction forming chain-line patterns which could coalesce to form nanorods. We believe that a molecular dynamics study

could throw more light on the details, but this is outside the scope of the present experimental work.

Photocatalytic activity

The photocatalytic activity measurement for the hydrogen evolution from H₂S splitting under the visible light exposure was performed using the as-synthesized (γ -Fe₂O₃) α -Fe₂O₃ (core) shell nanorods synthesized at 450 °C (please refer to the XRD data of Fig. 1c) and α -Fe₂O₃ nanorods obtained by heating at 500 °C for 180 min with 15 °C per min heating rate (please refer to the XRD data of Fig. 1d). The core/shell nanorods showed enhanced photocatalytic hydrogen evolution (75 ml h⁻¹) as compared to the α -Fe₂O₃ nanorods case (60 ml h⁻¹) as well as our previous report (51 ml h⁻¹) on maghemite and hematite necked nanostructures.⁶ The surface area of our core/shell sample was found to be 66 m² g⁻¹, which is comparable to the values of 68 m² g⁻¹ and 61 m² g⁻¹, respectively, reported for the maghemite and hematite necked structures.⁶ The fact that the activity of our sample is still significantly higher implies the possible role of a different surface morphology (active site density) of the thin hematite shell in the core shell configuration. More work is needed to elucidate these aspects further.

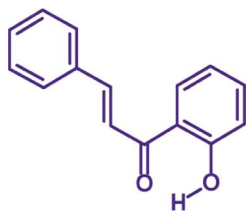
3. Experimental

3.1 Chemicals

All of the reagents used, such as ferrous ammonium sulphate, benzaldehyde, 2'-hydroxyacetophenone, NaOH and H₂SO₄ etc., were analytical grade.

3.2 Preparation of ligand

The 2'-hydroxychalcone (2'-HC) ligand was synthesized by condensation of benzaldehyde with 2'-hydroxyacetophenone in the presence of 10% NaOH in distilled water and absolute ethanol.³⁰ The product thus obtained was recrystallized by using ethanol. The molecular structure of the ligand is as shown below as Scheme 2.



Scheme 2 Structure of ligand (2'-hydroxy chalcone).

3.3 Preparation of iron complexes

The metal salt was used as a precursor for the preparation of the complex. Ferrous ammonium sulphate was used as source of Fe(II). 15 mmol solution of the ligand was made in 50 ml alcohol. To that 2 ml 1 N NaOH was added. This solution was then added under constant stirring into 5 mmol solution of salt of the metal ion in 100 ml distilled water. A few drops of dilute H₂SO₄ were added to avoid hydroxide formation of metal due to the presence

of NaOH. The product was filtered and washed 2–3 times using distilled water and finally by absolute ethanol to remove excess or unreacted ligand. The synthesized product was dried at RT for two days.

3.4 Preparation of iron oxide nanorods

The maghemite (hematite) core (shell) nanorods were synthesized via a simple but controlled thermal decomposition of [Fe(III) (2'-hydroxy chalcone)₃] complex. For this 1000 mg of complex was weighed in the alumina crucible and kept in the furnace which was then heated to a temperature of 450 °C. The changes in the final product were examined for a) different heating rates (1 °C, 10 °C and 15 °C per min) leading to 450 °C, and b) for different durations of heating (30, 90, 150, 180 min) at 450 °C for heating rate of 15 °C per min. The Fe-complex was also annealed at different temperature (375, 475 and 500 °C) for 3 h at a heating rate of 15 °C and the corresponding products were studied. In all cases furnace was cooled naturally. It is useful to mention here that for the optimized case of annealing at 450 °C for 3 h, the yield was 23 mg (which is 2.3% by wt. of the original complex). We verified that processing for 5 and 20 g of powder did not change the outcome in any significant way, suggesting the scalability.

3.5 Characterization

The synthesized powder samples were characterized by X-ray diffraction (XRD, Pananalytical model Xpert Pro), high resolution transmission electron microscopy and selected-area electron diffraction (HRTEM 300KeV Technai), field emission scanning electron microscopy (FE-SEM HITACHI S4800), and Mössbauer spectroscopy using ⁵⁷Co(Rh) γ -ray source and α -Fe foil as the standard for calibration. Room temperature UV-Vis-NIR absorption measurements were performed using Perkin Elmer Lambda-9 spectrophotometer. Magnetic properties were investigated by using a vibrating sample magnetometer with an applied field between ± 20 KOe at room temperature. Thermal study of the samples (ligand and Fe-complex) was done by using thermo-gravimetric analysis (SETARAM-16/18).

Photodecomposition of H₂S

The photocatalyst was introduced as a suspension into a cylindrical quartz reactor and a thermostat based water jacket. A xenon lamp light source (Oriel) with a power of 300 W and a cut off filter (>420 nm) was used. At a constant temperature the vigorously stirred suspension was purged with Ar for half hour. The experiment was carried out using 50 mg of catalyst in 200 ml of aq. KOH solution (0.5 M). The excess hydrogen sulphide was trapped in NaOH solution. The amount of evolved H₂ was measured using graduated gas burette and gas chromatograph (Model Shimadzu GC-14B, MS-5 Å column, TCD, Ar carrier).

4. Conclusions

In conclusion, we have studied the process of thermolysis of a molecular solid of a Fe-complex and have shown that it leads to the synthesis of maghemite (hematite) core (shell) nanorods. The materials are characterized using a variety of methods and an attempt is made to throw light on the possible mechanisms.

We believe that the molecular solid based low temperature solid–solid transformation route to inorganic phase synthesis may provide interesting opportunities for controlling the phase and constitution provided it can be used in conjugation with other functional precursors. Photocatalytic activity was also performed for hydrogen production from H₂S under solar light. Hydrogen evolution thus obtained (75 ml h⁻¹) is much higher as compared to the earlier report.

Acknowledgements

NC, SW and BBK are thankful to the Center for materials for electronics technology (C-MET) Govt. of India for funding support. SJ, BL, BH and SBO are thankful to the Indo-French center (CEFIPRA) for funding (grant no. 3808-2). Thanks are also due to Omkar Game for help with magnetization measurements.

References

- 1 C. C. Berry and A. S. D. Curtis, *J. Phys. D: Appl. Phys.*, 2003, **36**, R198.
- 2 J. G. Zhu, *IEEE Trans. Magn.*, 1993, **29**, 195.
- 3 I. Žutić and J. Fabian, *Rev. Mod. Phys.*, 2004, **76**, 323.
- 4 L. Meng, W. Chen, C. Chen, H. Zhou, Q. Peng and Y. Li, *Cryst. Growth Des.*, 2010, **10**, 479–482.
- 5 J. Park, B. Koo, K. Y. Yoon, Y. Hwang, M. Kang, J. G. Park and T. Hyeon, *J. Am. Chem. Soc.*, 2005, **127**, 8433–8440.
- 6 S. K. Apte, S. D. Naik, R. S. Sonawane, J. O. Baeg and B. B. Kale, *J. Am. Ceram. Soc.*, 2007, **90**, 412–414.
- 7 S. B. Wang, Y. L. Min and S. H. Yu, *J. Phys. Chem. C*, 2007, **111**, 3551–3554.
- 8 Y. Piao, J. Kim, Y. Jang, T. Hyeon and Angew, *Angew. Chem., Int. Ed.*, 2007, **46**, 7039–7043.
- 9 Y. Ding, J. R. Morber, R. L. Snyder and Z. L. Wang, *Adv. Funct. Mater.*, 2007, **17**, 1172–1178.
- 10 J. Chen, L. Xu, W. Li and X. Gou, *Adv. Mater.*, 2005, **17**, 582–586.
- 11 M. V. Reddy, T. Yu, C. H. Sow, Z. X. Shen, C. T. Lim, G. V. S. Rao and B. V. R. Chowdari, *Adv. Funct. Mater.*, 2007, **17**, 2792–2799.
- 12 R. M. Cornell and U. Schwertmann, in *The Iron Oxides*, Wiley-VCH, Verlag GmbH and Co. KGaA, Weinheim, 2nd edn, 2003.
- 13 T. Wang, Y. Wang, F. Li, C. Xu and D. Zhou, *J. Phys.: Condens. Matter*, 2006, **18**, 10545.
- 14 A. E. Kasmí, J. M. Wallace, E. F. Bowden, S. M. Binet and R. J. Linderman, *J. Am. Chem. Soc.*, 1998, **120**, 225.
- 15 H. Imahori, H. Norieda, H. Yamada, Y. Nishimura, I. Yamazaki, Y. Sakata and S. Fukuzumi, *J. Am. Chem. Soc.*, 2001, **123**, 100.
- 16 C. Sudakar, G. N. Subbanna and T. R. N. Kutty, *J. Mater. Chem.*, 2002, **12**, 107.
- 17 K. Kandori, M. Fukuoka and T. Ishikawa, *J. Mater. Sci.*, 1991, **26**, 3313.
- 18 Z. Zhong, J. Ho, J. Teo, S. Shen and A. Gedanken, *Chem. Mater.*, 2007, **19**, 4776–4782.
- 19 A. S. S. Brown, J. S. J. Hargreaves and B. Rijniersce, *Catal. Lett.*, 1998, **53**, 7.
- 20 S. Bhagwat, H. Singh, A. Athawale, B. Hannover, S. Jouen, B. Lefez, D. Kundaliya, R. Pasaricha, S. Kulkarni and S. B. Ogale, *J. Nanosci. Nanotechnol.*, 2007, **7**, 4294–4302.
- 21 H. Hsiang and F. S. Yen, *Ceram. Int.*, 2003, **29**, 1–6.
- 22 D. L. A. de Faria, S. V. Silva and M. T. de Oliveira, *J. Raman Spectrosc.*, 1997, **28**, 873–878.
- 23 O. N. Shebanova and P. Lazor, *J. Raman Spectrosc.*, 2003, **34**, 845–852.
- 24 G. V. M. Jacintho, P. Corio and J. C. Rubim, *J. Electroanal. Chem.*, 2007, **603**, 27–34.
- 25 J. Wang, Y. Ma and K. Watanabe, *Chem. Mater.*, 2008, **20**, 20–22.
- 26 E. V. Shevchenko, M. I. Bodnarchuk, M. V. Kovalenko, D. V. Talapin, R. K. Smith, S. Aloni, W. Heiss and A. P. Alivisatos, *Adv. Mater.*, 2008, **20**, 4323–4329.
- 27 T. Hyeon, S. S. Lee, J. Park, Y. Chung and H. B. Na, *J. Am. Chem. Soc.*, 2001, **123**, 12798–12801.
- 28 J. I. N. Qin-han and S. H. Guzar, *J. Appl. Sci.*, 2008, **8**, 2480–2485.
- 29 W. Coats and J. P. Redfern, *Nature*, 1964, **201**, 68.
- 30 J. M. Devi, P. Tharmaraj, S. K. Ramakrishnan and K. Ramachandran, *Mater. Lett.*, 2008, **62**, 852.